Contents lists available at ScienceDirect

Geothermics

journal homepage: www.elsevier.com

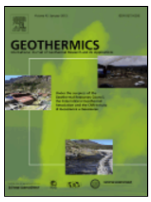

Deciphering origins and pathways of low-enthalpy geothermal waters in the unconventional geothermal system of Juchipila graben (Central Mexico)

Andrea Billarent-Cedillo [a], Gilles Levresse [b,*], Luca Ferrari [b], Claudio Inguaggiato [c,d], Salvatore Inguaggiato [e], Eliseo Hernández-Pérez [a], Antonio Hernández-Espriú [f], Fernando Corbo Camargo [b], Jaime Carrera Hernández [b], Alberto Arias-Paz [f]

[a] Posgrado en Ciencias de la Tierra, UNAM Campus Juriquilla Blvd. Juriquilla 3001, Querétaro, 76230, Mexico
[b] Centro de Geociencias, UNAM Campus Juriquilla Blvd. Juriquilla 3001, Querétaro, 76230, Mexico
[c] Departamento de Geología, Centro de Investigación Científica y de Educación Superior de Ensenada (CICESE), Carretera Ensenada-Tijuana 3918, Ensenada, Baja California, Mexico
[d] Istituto Nazionale di Geofisica e Vulcanologia, Sezione di Bologna, Via Donato Creti 12, Bologna, Italy
[e] Istituto Nazionale di Geofisica e Vulcanologia, Sezione di Palermo, via Ugo La Malfa, 143, 90145, Palermo, Italy
[f] Hydrogeology Group, Facultad de Ingeniería, UNAM, Circuito Escolar 04360, C.U., 04510, Ciudad de Mexico, CDMX, Mexico

ARTICLE INFO

Keywords:
Hydrogeochemical processes
Helium isotopes
water stable isotopes
Unconventional geothermal system
Mexico

ABSTRACT

This work presents hydrochemical results for groundwater and dissolved gas samples collected from a thermal and cold aquifer in the Juchipila Basin, in southern Sierra Madre Occidental, central Mexico. Thermal springs in the Juchipila Basin reach temperatures of 60°C, these manifestations are not related to recent or active volcanism as are all the known geothermal fields in Mexico. The thermal waters (>32°C) are Na-HCO_3 and Na-SO_4 type, with an anomalous concentration of F, B, Li, and As. Their chemistry likely results from water-rock interaction processes. The cold waters (<32°C) have a Ca-HCO_3 composition typical of recent infiltration and shallow flow, but they have an anomalous concentration of NO_3. The δ^2H and $\delta^{18}O$ indicate a common meteoric source for the warm and cold water plotting along an evaporation line. The waters have higher CO_2 and He concentrations than the air-saturated water. The helium composition is mainly atmospheric and terrigenous with a mantle helium contribution of up to 14%. This suggests that faults affecting the region are deeply rooted, permitting mantle helium uprise. Geothermometry gives mean reservoir temperatures of 58-102°C. Based on these results, we propose a model of hydrothermal circulation in Juchipila Basin, in which rainwater infiltrates deeply through the graben edge fault system, dissolves ions and crustal helium, incorporates mantle helium, while heated by the geothermal gradient, and eventually surges and mixes with the cold, shallow aquifer along faults cutting the whole succession within the graben.

1. Introduction

Geothermal energy is an important renewable energy source with a wide range of uses, such as the production of electricity, greenhouses, and building heating and cooling systems (Fridleifsson, 2001; Lund et al., 2005). Geothermal research traditionally focuses on conventional fields associated with recent and active volcanic systems (e.g.,Hermanska et al., 2020). In Mexico, these include the fields of Los Azufres, Los Humeros, and Las Tres Vírgenes (e.g., Bruhn et al., 2020). Others like the giant Cerro Prieto field in Mexico and the Salton Sea field in the US, are closely related to magma intrusion in pull-apart basins located along the plate boundary, which provide a high heat flux (Gutierrez-Negrin et al., 2015). Although Mexico still has a number of conventional geothermal sites that can be potentially developed (Gutiérrez-Negrîn., 2019), the need to increase the production of dispatchable clean energy requires exploring also novel, unconventional geothermal prospects.

Medium to low-enthalpy hydrothermal manifestations unrelated to Pleistocene-Holocene volcanism have been studied only marginally in Mexico (Wolaver et al., 2013; Morales-Arredondo et al., 2018), whereas their geothermal potential and genesis remain unknown. This is the case for some Oligocene to early Miocene grabens in central-western Mexico, located away from the active volcanic arc.

* Corresponding author.
Email address: glevresse@geociencias.unam.mx (G. Levresse)

https://doi.org/10.1016/j.geothermics.2021.102076
Received 13 August 2020; Received in revised form 22 February 2021; Accepted 25 February 2021
Available online xxx
0375-6505/

The Juchipila graben hydrothermal system is an example of an unconventional reservoir, located south of the city of Zacatecas (Fig. 1B), which contains at least a dozen thermal springs and groundwater discharge zones with temperatures up to 60 °C distributed along a 150 km-long graben.

Hydrothermal activity in this area has not been explained to date. Extensional tectonics and felsic magmatism in the area are Oligocene to early Miocene (Ferrari et al., 2013, 2018) and a minor reactivation of the southern part of the graben, associated with mafic volcanism, took place in late Miocene (Martínez-Reséndiz, 2020). Consequently, the thermal anomaly cannot be associated with a cooling magma intrusion in the upper crust or with lithosphere thinning.

During the exploration and assessment of geothermal resources, geochemical and isotope tracers are used to get insights into the reservoir fluid and rock chemistry, the reservoir permeability and temperature, the groundwater flow direction, and the rates of water recharge into the reservoir (Giggenbach, 1992; Arnórsson, 2000; Arnorsson et al., 2007; Spycher et al., 2011; Battistel et al., 2014). The stable isotope composition of water (δ^2H and $\delta^{18}O$) is widely used as a tracer to determine the origin of groundwater, for assessing the degree of water-rock interaction, and as an indicator for mixing of waters from different sources (Arnórsson, 2000; Boschetti, 2013; Battistel et al., 2016). The isotope composition of noble gases, in particular He and Ne, helps to distinguish between the atmospheric, magmatic, and crustal contribution of these gases to the groundwater system (Sano and Wakita, 1985; Kipfer et al., 2002).

In this study, we propose an integrated hydrothermal model derived from the analysis of the geochemical properties from groundwater wells and thermal springs of the Juchipila Basin. Based on the chemical and isotope composition of the water, also including dissolved gases and He isotopes, we determine the origin of cold and thermal fluids, we suggest a possible heating mechanism and we identify possible water flow pathways.

2. Stratigraphic and structural framework of the Juchipila Basin

The Juchipila Basin is located in the southeastern part of the Sierra Madre Occidental (SMO) volcanic province, near its boundary with the Mesa Central (MC) physiographic province (Fig. 1A; Ferrari et al., 2007). The SMO is one of the largest felsic volcanic provinces of the world (Ferrari et al., 2007) and consists mainly of ignimbrites with less rhyolitic domes and fissural basaltic flows, formed mostly in two main pulses at ~33 to 29 Ma and 24 to 20 Ma. The SMO felsic province covers the Late Cretaceous to Eocene magmatic arc and older Mesozoic to Paleozoic volcano-sedimentary and metamorphic terranes (Ferrari et al., 2018).

The Juchipila Basin is hosted in the Juchipila-Tabasco and Calvillo grabens (Fig. 2), extensional tectonic structures formed in the late Oligocene-early Miocene (Ferrari et al., 2013, 2018). Its northern boundary approaches the ESE-WNW trending San Luis-Tepehuanes crustal fault system (SLT FS) (Fig. 1B; Nieto-Samaniego et al., 2005; Loza-Aguirre et al., 2008). To the south of the Juchipila graben is the Late Miocene-Quaternary Trans-Mexican Volcanic Belt (TMVB) (Ferrari et al., 2013). The TMVB volcanism has migrated southward so that the currently active volcanic centers and geothermal fields are found ~80–100 km south of the Juchipila Basin (Fig. 1A).

The local stratigraphy consists of a volcano-sedimentary succession made of 1) Eocene sandstone, felsic ignimbrites, and andesitic lavas flows that are cut by the main graben faults; 2) Oligocene felsic ignimbrites, rhyolitic domes, intraplate basaltic lava flows, and early Miocene sandstone and fluvial conglomerate emplaced during the graben formation; 3) middle to late Miocene basaltic lavas and late Miocene to early Pliocene lacustrine sediments with thickness up to 300 m, mostly exposed in the southern half of the graben (Martínez-Reséndiz, 2020).

The aquifer geometry is controlled by NNE-SSW extensional faults systems that bound the graben and by the accumulation of intra-graben ignimbrites that segment the basin in the northern and southern sections (Fig. 2). In the northern section, the Juchipila graben branches into the Calvillo and Tabasco grabens (Fig. 2). These grabens experienced an elongation of ~8%, and the major faults have a vertical displacement up to 1 km (Nieto-Samaniego et al., 1999).

According to the National Water Commission, CONAGUA (2018), the Juchipila area hosts an unconfined granular aquifer consisting of Miocene to Pliocene conglomerate and lacustrine sediments, and a fractured aquifer in the Oligocene volcano-sedimentary succession. In some areas of the southern part of the graben, the granular aquifer may be considered semiconfined due to the presence of rich-clay and calcareous layers within the lacustrine deposits (Fig. 2; CONAGUA, 2018).

3. Material and methods

3.1. Groundwater sampling

Forty-nine groundwater samples were collected from springs, shallow (< 25 m) and deep boreholes (25-300 m) at the dry and rainy seasons, during three surveys that lasted from 2017 to 2019. Physical-chemical parameters (temperature, pH, electrical conductiv-

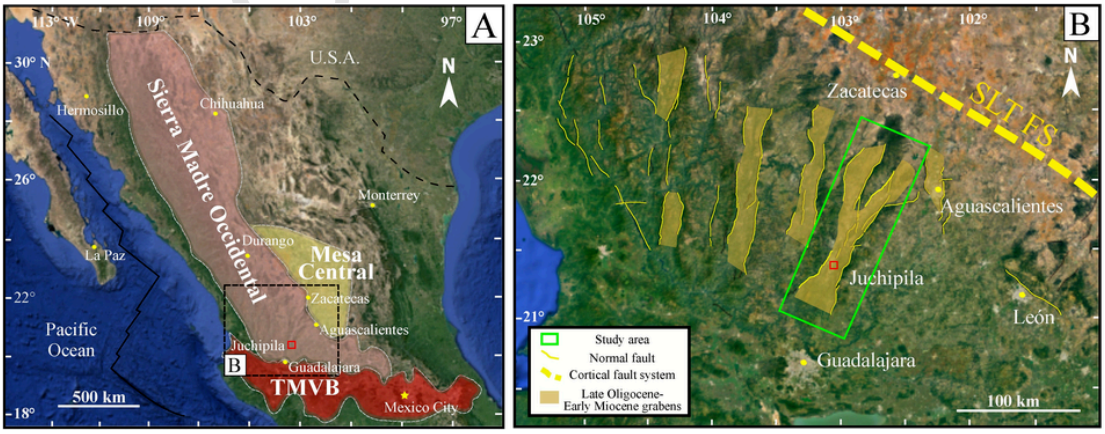

Fig. 1. Study area location. A: physiographic provinces in central and northwestern Mexico. B: Juchipila Basin location and the major structures in the southern portion of the SMO. SLT FS: San Luis-Tepehuanes crustal Fault System.

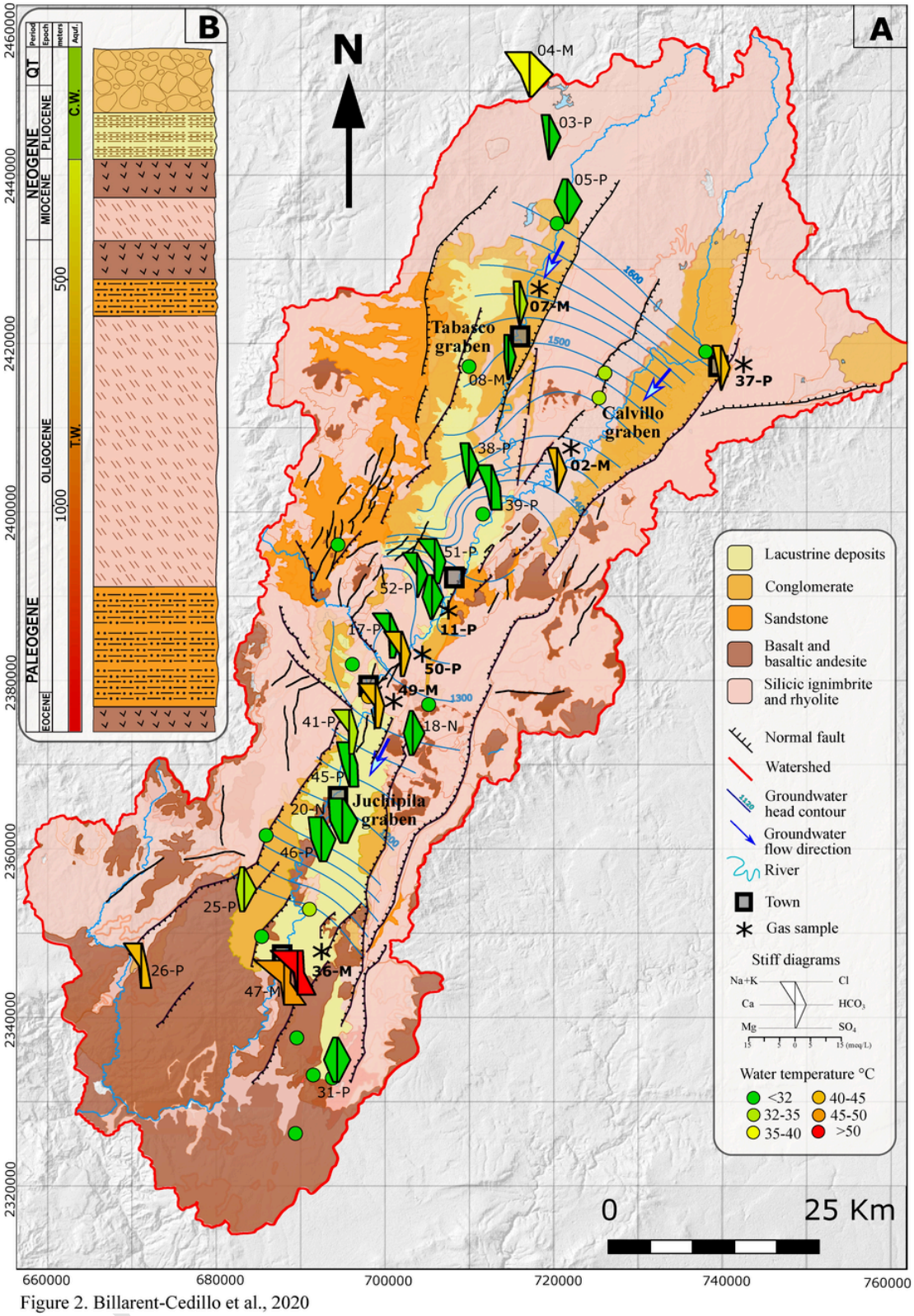

Figure 2. Billarent-Cedillo et al., 2020

Fig. 2. A. Simplified geological map of the Juchipila Basin. We present the location of water samples (dots) and Stiff diagrams from the Juchipila Basin. The geology of the basin is a simplified version from Martínez-Reséndiz (2020) and Beltrán-Martínez (2019). The color scale of the dots and Stiff diagrams correspond to the temperature of the samples. Stiff diagrams are labeled with the sample name by its side. The location for dissolved gas and He isotopes have a * by its side. The groundwater head contours and flow direction is taken from Paz-Pérez (2019). The flow direction (NE-SW) is pointed by blue arrows. B. Simplified stratigraphic column of the Juchipila Basin modified from Martínez-Reséndiz (2020). An approximate location of the C.W. and T.W. aquifers is shown.

ity, total dissolved solids, oxidation-reduction potential, and dissolved oxygen) were measured in situ using a *Thermo® Orion 5-Star Plus* multiparameter analyzer calibrated before sampling. Carbonate and bicarbonate alkalinity was also determined in situ with a Hach® digital titrator using H_2SO_4 0.16 M as a titrating reagent and methyl orange and phenolphthalein as indicators. All water samples were filtered in the field with 0.45 μm *Millipore®* cellulose acetate membrane filters and stored in high-density polyethylene bottles for dissolved anions and $\delta^{18}O$-$\delta^{2}H$ isotope analysis. In addition, samples for cation analysis were acidified to pH ~ 2 with ultrapure HNO_3. These samples were refrigerated until their arrival in the laboratory.

Seven water samples were collected in ~121 mL glass bottles to analyze for dissolved gases and helium isotopes (Capasso and Inguaggiato, 1998; Inguaggiato and Rizzo, 2004). The glass samplers were filled with water and sealed underwater with rubber septa to avoid air contamination during the sampling procedure. The method used to analyze for dissolved gases is based on the equilibrium partition of gases between the water phase collected and the gas phase (Capasso and Inguaggiato, 1998; Inguaggiato and Rizzo, 2004). The sample bottles were immersed in water to avoid air contamination during the storage time.

3.2. Analytical methods

Water was analyzed at the Laboratorio de Geoquímica Ambiental at the Centro de Geociencias, UNAM. Dissolved anions (F^-, Cl^-, NO_3^-, SO_4^{2-}) were determined by high-performance liquid chromatography/ion chromatography (HPLC/IC) with a *Dionex ICS-2500®* (precision ±2%). Dissolved cations (Na^+, Ca^{2+}, Mg^{2+}, K^+, Li^+, As_{tot}, Si^{4+}, B_{tot}) were determined by inductively coupled plasma optic emission (ICP-OES) with a *Thermo iCAP 6500 Duo View®. Quantification limits per element are given in Table 2.*

Water $^{18}O/^{16}O$ and $^{2}H/^{1}H$ isotopic ratios were analyzed for by isotope ratio laser spectrometry (IRLS) with a *Los Gatos Research DLT-100 V3®* at the Laboratorio de Isotopía Estable of the Instituto de Geología, UNAM. The samples were filtered through a 0.2 μm *Millipore®* cellulose acetate membrane before analysis. The isotope ratios are expressed in δ-notation (‰) normalized relative to the Vienna Standard Mean Ocean Water (VSMOW). The standard deviation for the $\delta^{18}O$ was less than ±0.2‰ and less than ±2‰ for the $\delta^{2}H$‰.

Dissolved gas and noble gas isotope analysis was performed at the geochemical laboratory of the Istituto Nazionale di Geofisica e Vulcanologia – Palermo (INGV-Pa). The chemical composition of dissolved gases was analyzed with an *Agilent 7890* gas chromatograph using Ar as the carrier gas. The gas chromatograph is equipped with two detectors: one of thermal conductivity (TCD) for the analysis of He, H_2, O_2, N_2, and another of flame ionization (FID) for the analysis of CO, CO_2, and CH_4. Further explanation of the method for gas extraction and dissolved gas analysis can be found in Capasso and Inguaggiato (1998). The analytical error was less than 5%.

The ^{3}He, ^{4}He, and ^{20}Ne isotopic concentrations were measured to calculate the $^{3}He/^{4}He$ and $^{4}He/^{20}Ne$ ratios using a noble gas mass spectrometer. Noble gases were purified from the gas mixture in a stainless steel ultra-high vacuum line and then cryogenically separated and admitted into a split flight tube noble gas mass spectrometer (*GVI® Helix SFT)* for He isotopes and into a multicollector noble gas mass spectrometer (*Thermo® Helix MC) for Ne isotopes*. A multicollector mass spectrometer (*GVI® Helix MC*) was used to analyze for Ar (Rizzo et al., 2015). The method for gas extraction and isotope analysis is described in detail in Inguaggiato and Rizzo (2004). The analytical error was less than 3% on a single mass determined. The concentration of dissolved gases is expressed as cm^3/g at 0°C and 1 atm (STP). The helium isotope ratios are reported as R/Ra, where R is the $^{3}He/^{4}He$ ratio determined in the sample, and Ra is the atmospheric one (1.39×10^{-6}). The R/Ra values were corrected for atmospheric contamination (Rc/Ra) using the air normalized $^{4}He/^{20}Ne$ ratio equation of Hilton (1996) :

$$\frac{R_C}{R_a} = \frac{\left(\frac{R}{R_a} * X\right) - 1}{X - 1} \quad (1)$$

$$\text{where } X = \frac{\left(\frac{He}{Ne}\right)_{sample}}{\left(\frac{He}{Ne}\right)_{air}} \frac{\beta_{Ne}}{\beta_{He}} \quad (2)$$

and β_{Ne} and β_{He} are the Bunsen solubility coefficients for Ne and He, respectively, at the temperature and salinity of the water when the atmospheric helium was dissolved.

4. Results

Physical-chemical parameters: temperature, pH, electrical conductivity (EC), total dissolved solids (TDS), oxidation-reduction potential (ORP), and dissolved oxygen (DO), as well as the isotope composition of water ($\delta^{2}H$ and $\delta^{18}O$), are presented in Table 1.

4.1. Water physical-chemistry

Overall, all sampling water temperatures are above the air mean temperature in the Juchipila Basin (~22 °C; Fig. 3). The temperature data show three distribution trends with breaking points at 32ºC and 50ºC (Fig. 3). The low-temperature wells and springs (22°-31 °C) represent the commonest and the most abundant water group (n = 33) in the Juchipila Basin (green symbols in Fig. 3). The second most represented group (n = 14) has temperatures from 32° to 50 °C (red symbols in Fig. 3). Finally, the highest temperature springs (> 60 °C), are only two, sample 36-M and 48-M (Fig. 3). Most springs and groundwater in the study area have a near-neutral pH (6.8–8.9). Water samples above 40 °C tend to be slightly more alkaline (7.6–8.8). Electric Conductivity (EC) values range from 327 to 1541 μs/cm; the low-temperature samples (< 32 °C) have an EC average of 595 μs/cm, the middle group samples (32 – 50°C) have an EC average of 686 μs/cm, and the high temperature (>60°C) samples an EC average of 1271 μs/cm. The majority of water samples are oxygen-rich, with positive ORP values ranging from 8 to 260 mV. The few samples with negative ORP values (-4 to -125 mV) correspond to well waters located in agricultural and livestock areas and to the springs with the highest temperature in the area (Fig. 2; Table 1).

The geographic distribution of water types through the Juchipila Basin (Fig. 2) indicates that warmer waters are restricted to the southern half of the basin and along the main graben faults. In contrast, colder waters commonly discharge in the valley. Considering the temperature distribution and its apparent correlation to other physical-chemical parameters, we decided to classify the waters into two groups: "cold" waters (CW) with sample temperatures < 32°C, and "thermal" waters (TW) with sample temperatures ≥ 32°C.

Major and trace elements measured in 25 of 41 recollected samples are presented in Table 2 and Fig. 4. All the presented samples have an ionic balance (IB) lower than ±11 %, indicating reliable data. Juchipila graben-related aquifer samples exhibit two main chemical water types: –HCO and Na-Ca–HCO to Na-Ca–2.2 ppm), As (0.03–0.21 ppm), Li (0.07–1.07 ppm), and F (0.3(1) The CW plot to Ca-Na-HCO_3 and Na-Ca-HCO_3-SO_4 water types, and (2) TW composition varies from Na-SO_4-HCO_3 to Na-Ca-HCO_3 types (Fig. 4). TW is also characterized by higher concentrations of B (0.1-2.2 ppm), As (0.03-0.21 ppm), Li (0.07-1.07 ppm), and F (0.3-12 ppm) than to the CW. CW presents a significant NO_3 concentration (up to 44 ppm)

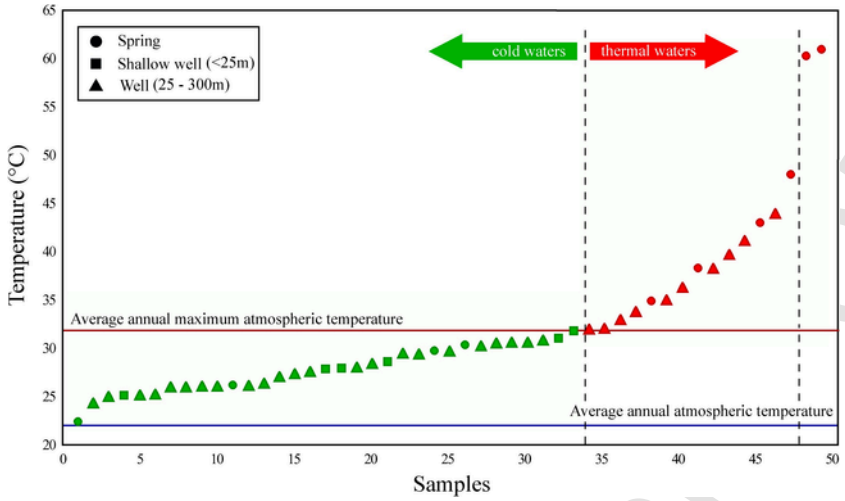

Fig. 3. Temperature distribution of water sampled from springs, shallow wells (< 25 m) and deep wells (25-300 m) in the Juchipila Basin. The blue line corresponds to the average annual athmospheric temperature and the red line to the average annual maximum athmospheric temperature (22 °C and 32 °C, respectively; CONAGUA, 2018).

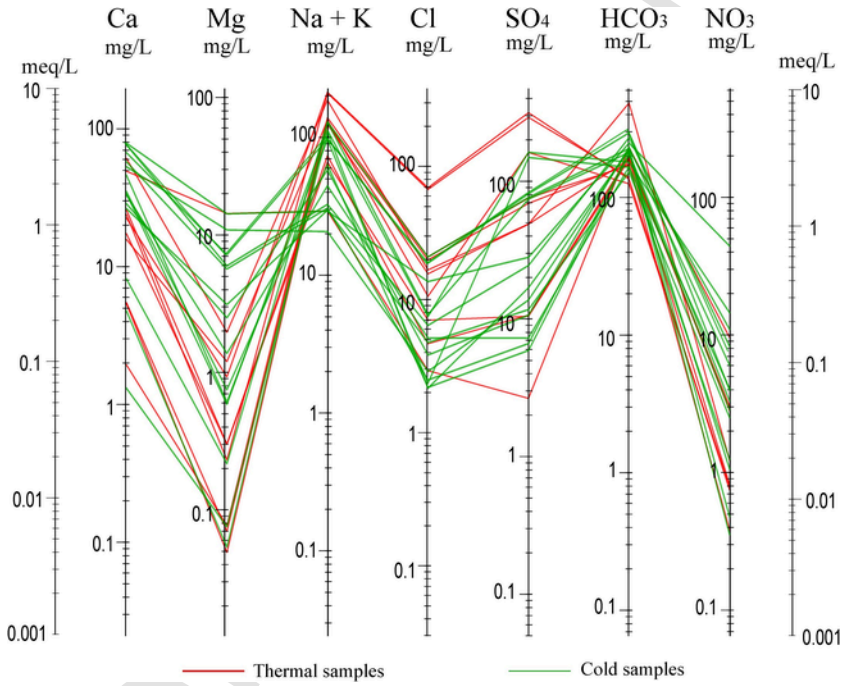

Fig. 4. Schöeller-Berkaloff diagram showing major ions of the water samples from the Juchipila Basin. Red lines correspond to the thermal samples and green lines to the cold samples.

compared to TW (up to 9.3ppm). Waters show an increase of TDS, Na, and SO_4 from north to south, parallel with the groundwater flow direction within the basin (Fig. 2).

4.2. Deuterium and oxygen stable isotopes

The δ^2H–$\delta^{18}O$ results for springs and well water are presented in Table 1 and Fig. 5. All isotope ratios in the Juchipila aquifer water range from -79.3‰ to -53.2‰ for δ^2H and -10.8‰ to -6.3‰ for $\delta^{18}O$. In the classical Craig's δ^2H–$\delta^{18}O$ diagram (Fig. 5), the isotope composition of waters from spring and well plots along a local evaporation water line (LEL: $\delta^2H = 5.5\ \delta^{18}O$ - 20), with a Global Meteoric Water Line intercept at -11.8‰ $\delta^{18}O$ and -85‰ δ^2H. Differentiated by temperature and chemistry, CW plots all along the LEL showing a larger evaporation grade than TW, with δ^2H ranging from -76.4‰ to -53.2‰, and $\delta^{18}O$ from -10.2‰ to -6.3‰; while TW samples are restricted and closer to the Global Meteoric Water Line (GMWL) intercept point, with δ^2H ranging from -79.3‰ to -72.2‰, and $\delta^{18}O$ from 10.8‰ to -9.7‰.

4.3. Gas chemistry and He isotopes

Detailed results for the dissolved gas chemistry and $^3He/^4He$ and $^4He/^{20}Ne$ isotope ratios are presented in Table 3, the samples locations are labeled in Fig. 2. In the Juchipila basin's water, N_2, CO_2, and O_2 are the predominant species, with concentrations ranging from 7.54 x 10^{-3} to 1.04 x 10^{-2} cm^3/g for the N_2, 4.85 x 10^{-4} to 2.44 x 10^{-2} cm^3/g for the CO_2, and 6.42 x 10^{-4} to 2.79 x 10^{-3} cm^3/g for the O_2. Samples have dissolved ^4He concentrations between 9.78 x 10^{-8} and 5.58 x 10^{-6} cm^3/g, and Rc/Ra values ranging from 0.07 to 1.36 (Table 3). There is no sharp distinction between CW and TW gas chemistry, but they display a certain geographic pattern. The dis-

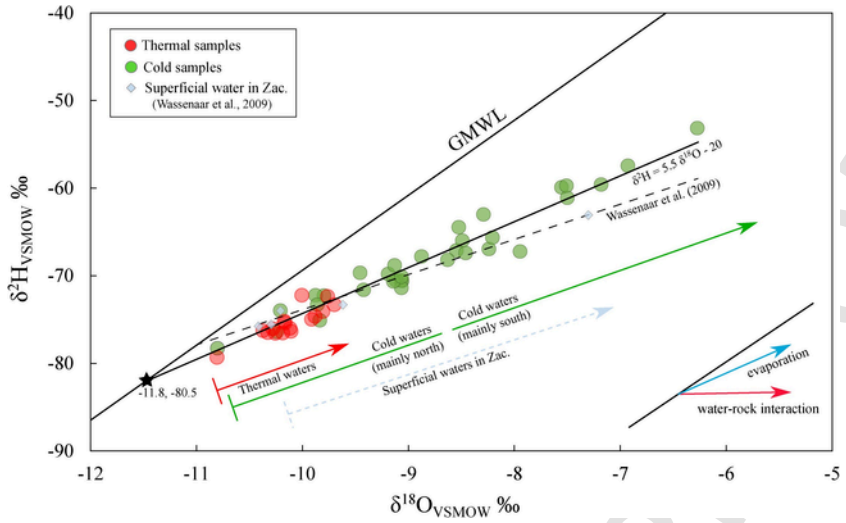

Fig. 5. D-O isotopic composition of the water samples from the Juchipila Basin (red and green dots) and of water samples from Zacatecas state (blue diamonds, Wassenaar et al., 2009). The evaporation line: $\delta^2H = 5.5\ \delta^{18}O - 19.3$ intercepts the GMWL ($\delta^2H = 8\delta^{18}O + 10$, Craig, 1961) at -11.8 ($\delta^{18}O$), -85 (δ^2H).

solved CO_2 concentration and the Rc/Ra values are lower towards the southern part of the basin, where the hottest samples are found (Fig. 6).

5. Discussion

5.1. Waters sources and hydrogeochemical processes

5.1.1. Water chemistry

The geology of the area controls the aquifer lithology while tectonics its geometry, which is reflected in the geographic pattern of the thermal and chemical features of the sampled waters (Fig. 7). The CW groundwater in the Juchipila aquifer follows an evolution trend inferred from the physicochemical parameters and chemical composition (Fig. 7). The main evolution path starts from a low-TDS, Ca–HCO_3^- composition, suggesting recently infiltrated water dissolving carbonates near the recharge zone and shallow flow (Chadha, 1999; Tóth, 1999). This water progressively evolves into a high-TDS, Na-SO_4-enriched group of TW due to the interaction with the host rocks, during plagioclase alteration processes. The evolution path has a north to south direction, paralleling the piezometric gradient of the shallow aquifer. In the southern part of the basin, a similar secondary evolution line goes in the opposite direction (from south to north).

The CW group is sourced from the local shallow granular aquifer of the graben (Fig. 2). The CW group in the northern part of the graben is mainly Ca-Na–HCO_3, with minor Na-Ca–HCO_3-SO_4 subtypes within the southern part (Stiff diagrams in Fig. 2, Fig. 7). This progressive enrichment in Na and depletion in Ca may be due to an ionic exchange process, very common in clay-rich sediments (Appelo and Postma, 2005), as water moves through the sediments in the valley from north to south. Besides, the anomalous concentrations of NO_3, in many cases accompanied by high Ca, Mg, and SO_4 (Fig. 4), indicate a mixture with irrigation run-off waters from many of the agricultural areas identified in the graben (Böhlke, 2002).

The TW group is sourced from the fractured aquifer within the volcaniclastic succession in the Juchipila Basin (Fig. 2); the Na predominance in this group points to a dissolution of plagioclase felspars from the volcano-sedimentary succession. Most TW samples are HCO_3-rich, such as CW (Fig. 4), but towards the southern part of the basin, they get enriched in SO_4 and Cl, suggesting an intermediate flow system (Mifflin, 1988; Tóth, 1999). Alternatively, this local SO_4 enrichment may be a consequence of evaporite dissolution or sulfur oxidation within the lacustrine deposits. According to Lahiere (1982), the fossil record in the Juchipila graben evinces a saline to hypersaline paleo-lake environment; thus evaporites may exist at

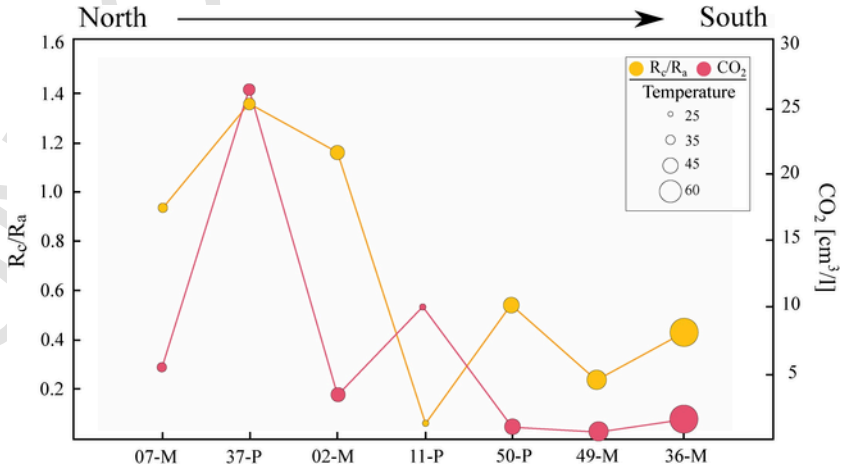

Fig. 6. North - south section of Rc/Ra ratios and CO_2 concentration of dissolved gas from TW and CW water samples in the Juchipila Basin.

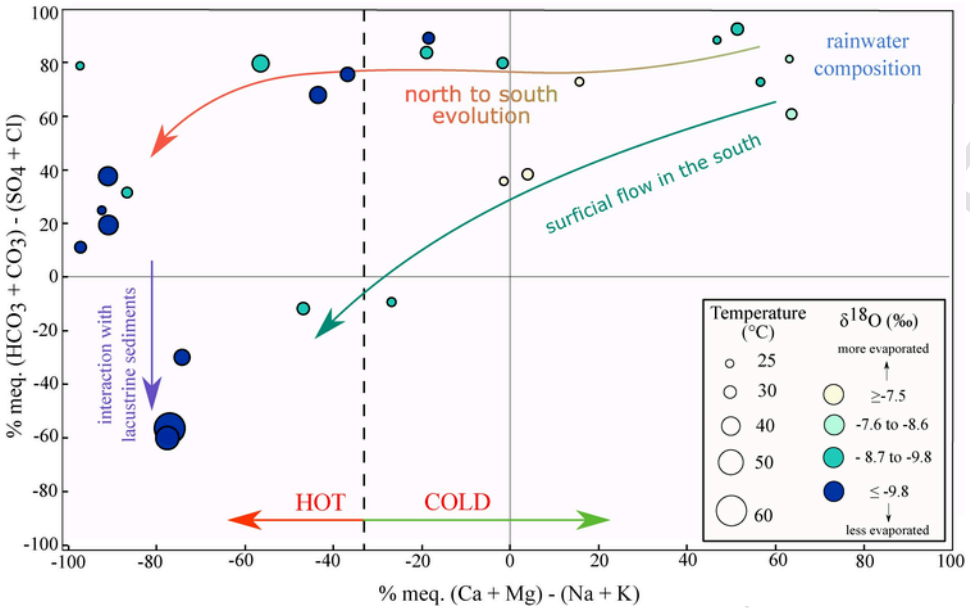

Fig. 7. Chadha diagram showing the temperature, chemistry, and isotopic evolution of samples from the Juchipila Basin. $\delta^{18}O$ is used as a magnitude of evaporation as it is more sensitive than $\delta^{2}H$.

depth, although not exposed at the surface (outcrops). TW samples from the southern portion of the basin have a $Ca/(Ca + SO_4)$ molar ratio < 0.5 (lower than the gypsum dissolution ratio = 0.5), implying a later Ca removal either by precipitation or ionic exchange. An anthropogenic influence in these waters is dismissed as an increment in NO_3 and Mg does not accompany the SO_4 enrichment in TW. Volcanic gas oxidation is also dismissed, no fumarole or bubbling waters were recognized. The disproportionation-hydrolysis of SO_2 and H_2S oxidation is usually coupled with very low pH values in volcanic – hydrothermal systems while the hot waters of Juchipila Basin have near-neutral pH (Delmelle and Bernard, 2015; Inguaggiato et al., 2017a).

The low reactivity and conservative character of Cl, Li, and B are useful for tracing alteration and dissolution processes in rocks (Giggenbach, 1991; Arnórsson, 2000). The higher proportion of B and Li compared to Cl in TW (Fig. 8) shows that alteration and dissolution are the major processes controlling the water chemistry. On the other hand, CW has a higher proportion of Cl and a deficit in B (Fig. 8); this high Cl may be due to manure and fertilizer contamination rather than natural processes (Böhlke, 2002; Rodvang et al., 2004). In addition, an anomalous concentration in (and the correlation between) B, Li, As, and F is observed in TW group, in some cases higher than the maximum limit for drinking water established in the

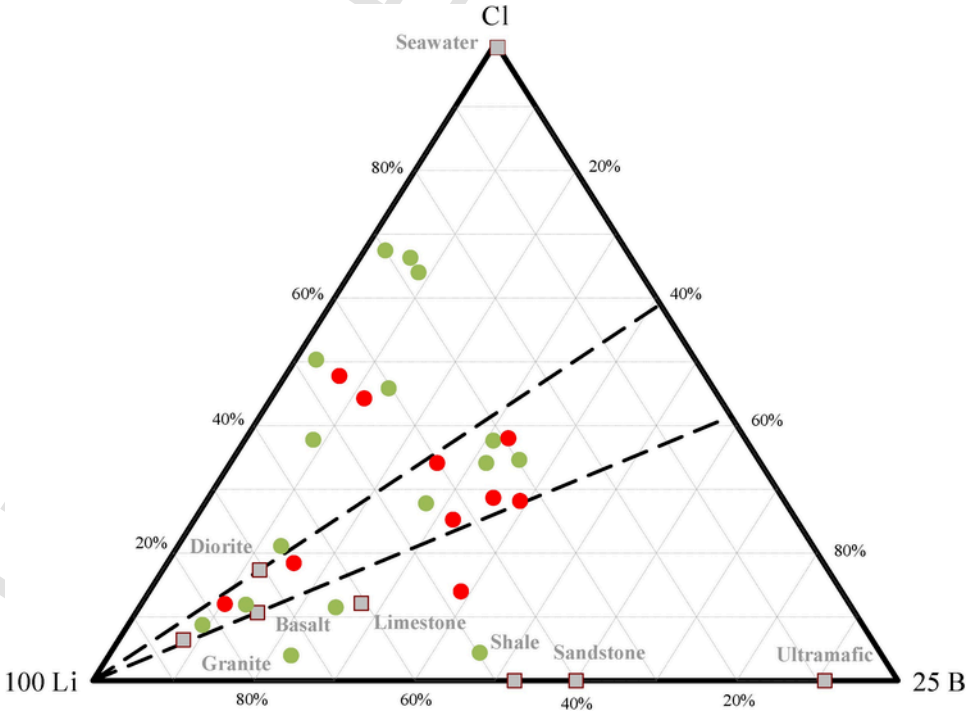

Fig. 8. 25B-100Li-Cl ternary diagram (Giggenbach, 1991). Red dots are TW samples and green dots are CW samples.

official norm in Mexico. These anomalies indicate that alteration and dissolution of the ignimbrite and rhyolite minerals and volcanic glasses provide most of these ions, as has been documented in other ignimbrite-related groundwater systems (Shaw and Sturchio, 1992; Nicolli et al., 2012; Alarcón-Herrera et al., 2013).

In summary, the chemistry of the TW group is dominated by interaction processes with volcanic rocks, while the chemistry of the CW group is dominated by shallow processes such as water interaction with soil materials, intra-graben sediments, and manure and fertilizer contamination.

5.1.2. δ^2H–$\delta^{18}O$ composition

In the δ^2H–$\delta^{18}O$ diagram (Fig. 5), the isotopic composition of all springs and borehole waters plot along a common regression line (LEL: $\delta^2H = 5.5\ \delta^{18}O - 20$).

CW samples plot along the whole line, while TW samples have more negative values and a restricted distribution closer to the GMWL. Such linear distribution is generally interpreted as a two end-member mixing or an evaporation processes. The intersection of the regression line with the GMWL is considered representative of the initial meteoric water δ^2H-$\delta^{18}O$ composition (Craig et al., 1963). Considering a typical andesitic water composition (δ^2H between -30‰ and -10‰, and $\delta^{18}O$ between 8‰ and 10‰; Giggenbach, 1992), the low δ^2H and $\delta^{18}O$ values for all samples preclude any mixture with volcanic water. This is an opposite behavior to that of the conventional geothermal well and spring samples from the volcanic-related fields of Mexico (Pinti et al., 2013, 2019). The distribution of the isotope values from shallow wells (5–20 m) in Zacatecas state (Wassenaar et al., 2009) overlaps the Juchipila aquifer isotopic trend and suggests that evaporation is the main process controlling the δ^2H-$\delta^{18}O$ isotopic distribution.

Considering an evaporation line, CW located in the southern part of the study area shows a higher evaporation rate loss than samples in the north and along the graben edge (Fig. 5). This N–S trend in the CW isotope composition follows the topographic gradient (such as the flow direction of the shallow aquifer) and reflects superficial run-off processes, namely significant evaporation of rainwater before infiltrating into the soil. Considering only the samples selected for chemical analysis, the increasing evaporation has an opposite relation with the chemical evolution and Na and SO_4 enrichment (Fig. 7). In contrast, TW seems less affected by superficial run-off and evaporation processes. The narrow range and low d^2H and $d^{18}O$ values for this group suggest a rapid infiltration process or a vertical recharge from precipitation, and the existence of another (deeper) flow system. The apparent contradiction of a meteoric-like stable isotopic composition of water with enrichment of Na and SO_4 due to water-rock interaction could be explained by the rapid infiltration of meteoric water into the fractured felsic ignimbrites. This meteoric water with a mean temperature of 18°C-22°C and neutral pH may have the potential to dissolve carbonate and some silicate phases as plagioclase, but not the oxides as quartz, which represents the main magmatic oxygen source in the ignimbrite mineralogy. Also, the meteoric versus alteration oxygen ratio is probably too high to illustrate a potential isotopic variation (within the margin of error) (Fig. 7).

To sum up, in the Juchipila graben, all waters sampled have a meteoric origin. The isotopic variability responds to the infiltration processes, and the differences in chemistry reflect the interaction with the distinct host rocks of each flow system.

5.2. Origin of gases and relationship with the thermal source

5.2.1. Dissolved gas chemistry

Thermal manifestations, such as free gases and bubbling gases, are not always easily identifiable at a field level. At the surface, gas manifestations may be hidden; still, we can find gases dissolved in groundwater as a function of their solubility. Gases dissolved in water can reflect the gas-water interaction with other fluids rather than the air, providing valuable information on the nature of the fluids and their relation with the geodynamic context or local tectonic setting (Capasso and Inguaggiato, 1998; Caracausi et al., 2004; Kulongoski et al., 2013; Inguaggiato et al., 2016, 2017b; Arnold et al., 2020).

The relative proportion of CO_2, N_2, O_2 were plotted in a triangular plot (Fig. 9) and compared with the air-saturated water composition (ASW). The samples are characterized by a CO_2 enrichment with respect to the ASW. This evidence allows us to propose that sampled groundwaters also interact with non-atmospheric CO_2. For instance, sample 37-P, located in the northern part of the area, has the highest CO_2 concentration (2.44×10^{-2} cm^3/g), one order of magnitude higher than the remaining samples (Fig. 6). Dissolved He concentrations are one or even two orders of magnitude higher than in ASW ($[He]_{ASW} = 4.58 \times 10^{-8}$ cm^3/g, Smith and Kennedy, 1983), suggesting an interaction with He-enriched fluids from a different source than air; the He source will be discussed in the next section. Dissolved gases determined have lower N_2/Ar ratios than the ASW ($N_2/Ar = 38$), ranging from 18.3 to 36.2, indicating a negligible contribution of magmatic or crustal/organic N_2 (Giggenbach, 1980; Norman and Moore, 1999; Inguaggiato and Rizzo, 2004; Fischer and Chiodini, 2015).

5.2.2. He isotopes

In a hydrothermal system, helium isotopes can be used as geochemical tracers to identify the sources of He and fluids carrying it, namely meteoric waters carrying atmospheric He, groundwater carrying crustal He and "magmatic" aqueous fluids, or deep-seated gases carrying mantle He (Kennedy and van Soest, 2007; Kulongoski et al., 2013; Inguaggiato et al. 2016; Batista et al., 2019). The isotope composition of dissolved He in water is thus a mixture of that of the atmospheric, mantle, and crustal helium isotopic end-members (Sano and Wakita, 1985). In this study, we considered the air-saturated water (ASW) end-member instead of the atmospheric one, as the helium determined comes from dissolved gas samples and not from free or bubbling gases.

The R/Ra ratio versus the $^4He/^{20}Ne$ ratio for each sample is plotted in Fig. 10. The end-members were plotted for comparison. Most of the samples fall relatively close to the ASW end-member, even if significant crustal and mantle contributions are easily recognized.

The contribution of each end-member (Table 3) was calculated following the equation system developed by Sano and Wakita (1985):

$$\frac{R}{Ra} = A\frac{R}{Ra}_{ASW} + M\frac{R}{Ra}_{m} + C\frac{R}{Ra}_{c} \quad (3)$$

$$1/\frac{^4He}{^{20}Ne} = A/\frac{^4He}{^{20}Ne}_{ASW} + M/\frac{^4He}{^{20}Ne}_{m} + C/\frac{^4He}{^{20}Ne}_{c} \quad (4)$$

$$A + M + C = 1 \quad (5)$$

where A, M, and C represent the atmospheric, mantellic, and crustal He components, respectively. The end-members used for the calculations are: $^4He/^{20}Ne$ ratios of 0.265 for ASW (Smith and Kennedy, 1983), and 1000 for crustal and mantle fluids (Craig et al., 1978; Sano and Wakita, 1985); and the R/Ra ratios of 0.983 Ra for ASW (Benson and Krause, 1980), 0.02 Ra for the crust (Hooker et al., 1985), and 7.3 Ra for the lithospheric mantle beneath Mexico (Straub et al., 2011). %–78 %–61 The Juchipila hydrothermal system has a predominant contribution from the ASW end-member (23%-72%) and the crustal end-member (25%-63%). The mantle he-

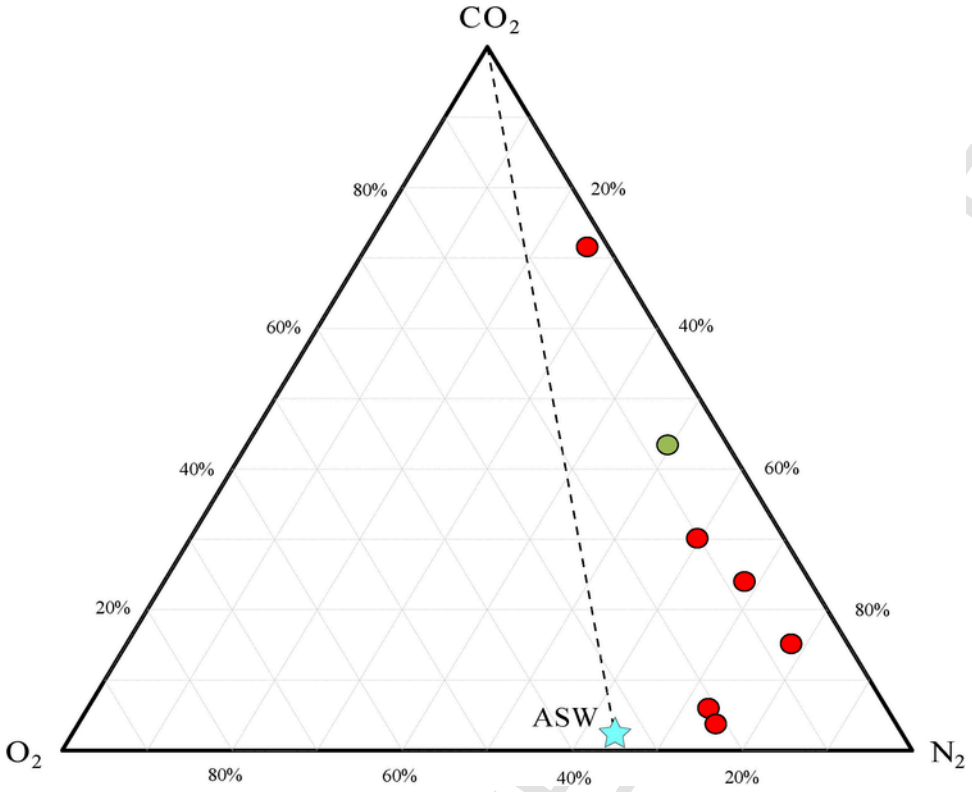

Fig. 9. CO_2-N_2-O_2 ternary diagram for dissolved gas samples. The green dot is a CW sample, red dots are TW samples, and the star is the composition of the ASW.

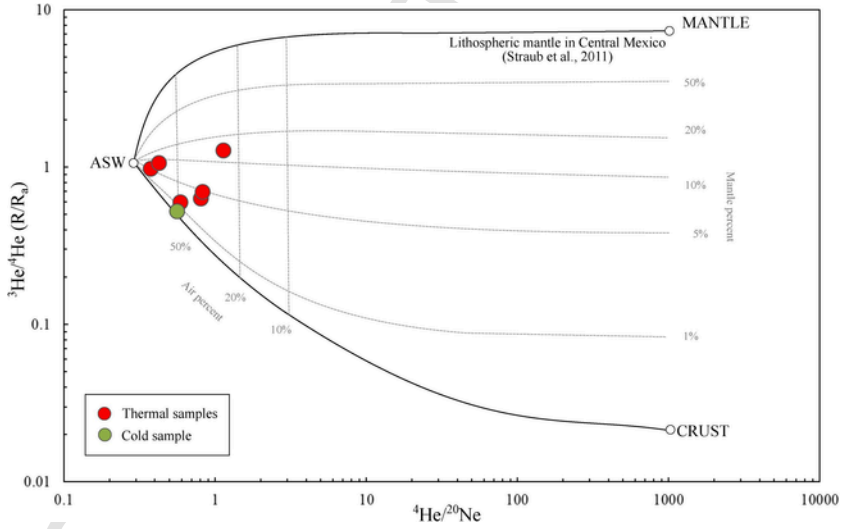

Fig. 10. R/Ra vs. $^4He/^{20}Ne$ plot for helium isotopic composition. Mantle, crust, and ASW end-members, as well as the mantel and air percentages, are shown. The $^4He/^{20}Ne$ end-member ratios used are 0.265 for ASW (Smith and Kennedy, 1983), and 1000 for crustal and mantellic fluids (Sano and Wakita, 1985). The R/Ra end-member ratios used are 0.983 Ra for ASW (Benson and Krause, 1980), 0.02 Ra for the crust (Hooker et al., 1985), and 7.3 Ra for the lithospheric mantle in Mexico (Straub et al., 2011).

lium contribution is lower than that of the other end-members but reaches values up to 14 %. R/Ra values were corrected for any atmospheric component. Resulting Rc/Ra values for the Juchipila TW aquifer are above the crustal radiogenic ratio of 0.02Ra (Hooker et al., 1985), suggesting the presence of mantle-derived fluids in the aquifer water. High Rc/Ra are found in the samples located in the northern part of the graben (Fig. 6), distributed along or close to the major faults defining the so-called Calvillo and Tabasco grabens (Fig. 2).

Particularly, the water sample 37-P located along the Calvillo graben has the highest Rc/Ra value (with a 14 % of mantle-He contribution) and 2.44 x 10^{-2} cm^3/g of CO_2 (Fig. 6). Low Rc/Ra values were measured in groundwater wells and springs from the valley in the central and southern part of the graben (Fig. 6), where the sediment filling is thicker (at least double) than in the north. This distribution suggests that mantle-derived fluids ascend preferentially in the northern part of the graben or, alternatively, that the dilution within the shallow aquifer is more significant in the southern part of the graben. The lack of a Quaternary shallow magmatic system in the area suggests that the high Rc/Ra values in the northern part of the basin are due to either 1) interaction between groundwater and volcanic rocks (or blind intrusives), specifically mineral dissolution and

diffusive exchange processes; 2) the invasion of geo-pressured fluids degassed from mantle melts enhanced by crustal permeability in proximity to the regional fault systems (Kennedy and van Soest, 2006); or 3) a combination of the two previous hypothesis.

% ()–8.4 ppm and 2To test the first hypothesis, we used a magma aging model proposed by Torgersen and Jenkins (1982), which suggests that an unusually gas-rich magma may be responsible for a long-lasting presence of a mantle helium component in the crust. The equation describing this model estimates the initial $^3He/^4He$ ratio in the magma source (Rc/Ra_{init}) by (Méjean et al., 2020): where Rc/Ra_{fin} is the measured Rc/Ra in the groundwater system, $^4He_{init}$ is the amount of ^4He in the magma source at t = 0, t is the age of the magma source, and J_{4He} is the ^4He production rate (in $cm^3STP/g/yr$) calculated following the equation (Torgersen et al., 1995) : where [U] and [Th] are the concentrations of U and Th in the rock in ppm. In the Juchipila basin, the U and Th concentration in the Oligocene (t = 30 Ma) volcano-sedimentary sucession range from 1.2 to 8.4 ppm and from 2 to 38.2 ppm respectively (Table 4; Martínez-Resendiz, 2020).

For the Rc/Ra_{fin} parameter, we used the maximum Rc/Ra value measured in the basin (1.36 Ra) corresponding to the 37-P sample, located in the graben shoulder (cutting only the volcano-sedimentary succession). To have a more robust approach, we used three values for the potential $^4H_{init}$: 1) 6.7 x 10^{-6} cm^3/g for a ^4He enriched magma, MORB-like source or proxy for a hotspot source (Torgersen et al., 1995); 2) 6.7 x 10^{-7} for a low-initial $^3He/^4He$ subduction zone magma (Torgersen et al., 1995); and 3) 2.84 x 10^{-8} as a proxy of a subduction zone magma in the TMVB according to the ^4He measured in olivines from the Pleistocene to present Trans Mexican Volcanic Belt (TMVB; Straub et al., 2011). The Rc/Ra_{init} values vary following the magmatic sources from: 1) 6.1 to 12.9 with a mean value of 9.4 ± 2.0; 2) 48.8 to 118 with a mean value of 82.2 ± 20.0; and 3) 1118.3 to 2739 with a mean value of 1906.4 ± 470.3 (Table 4). The Rc/Ra_{init} calculated for the magmatic sources using input parameters 2) and 3) are unrealistically high (with means of 102 ± 81.3 and 2371.4 ± 1914.6 respectively), indicating that the magma aging model considering subduction zone magmas is not able of explaining the mantle helium signature in the Juchipila reservoir. The range of Rc/Ra_{init} value (6.1 to 41) obtained from parameter 1) suggests that the He may be locally produced by aging and leaching processes. However, some geological observations do not conform to the aging hypothesis. Magmatism in the Juchipila area is the product of a subduction process (Ferrari et al., 2013); this process has occurred for the last 90 Ma, possibly leading to a He depletion in the mantle wedge up to one order of magnitude compared to the MORB average (according to the He concentrations reported by Straub et al., 2011). Additionally, in the Juchipila graben, the borders and the filling graben rocks are the same Oligocene ignimbrite. Even if aging is the same in both areas, the leaching process is more efficient in granular than fractured rocks, as the contact surface is significantly larger. For this reason, it would be expected to have higher Rc/Ra ratios within the graben fill, rather than in the fault traces. Also, CW and TW waters have neutral pH and are relatively "cold" compared to classic hydrothermal waters. As previously stated, the alteration process is not aggressive enough to significantly modify the meteoric oxygen isotopic signature, and the same behavior should be expected for the He isotopic ratios. Furthermore, the structural control and the N-S depletion in the Rc/Ra ratios suggest the existence of fluids degassed from upper mantle melts (present intrusions; Aranda-Gomez et al., 2007) along with the limits of the geologic provinces, such as the Tepehuanes Fault System. With these considerations, the geological and geochemical evidence, we propose that the mantle He signal in the Juchipila basin is related to degassing (during partial melting) of undetected present magma intrusions associated with the deep faults bounding the graben, as well as its proximity to the boundaries between the SMO and MC crustal provinces (Fig. 1). Mantle-derived He in the Juchipila Basin could be transported by a regional flow system facilitated by the intersections between the crustal-scale fault systems. The Juchipila hydrothermal system is very similar to some other hydrothermal and geothermal non-magmatic systems in North America. Rc/Ra values in our area are slightly higher than those for fluids in the Basin and Range (Raft River: 0.13 – 0.17 Ra, Torgersen and Jenkins, 1982; Dixie Valley: 0.7 - 0.8 Ra, Kennedy and van Soest, 2006), and slightly lower than that for fluids in the Sierra Madre Oriental and the Trans Mexican Volcanic Belt (TMVB) (Cuatro Ciénegas Basin: 0.89 – 1.85 Ra, Wolaver et al., 2013; Geysers field: 0.91 – 1.74 Ra, González-Guzmán et al., 2019). The dynamics of these systems are controlled by basement-penetrating faults allowing a deep circulation of fluids, most of them in high heat flow areas.

5.2.3. Geothermometry

The reservoir temperature was estimated using solute geothermometry in an attempt to constrain better the hydrothermal depth and the dynamics of the TW group. Solute geothermometry has been widely used to estimate subsurface temperatures in geothermal systems since earlies '60 s (D'Amore and Arnórsson, 2000, and references therein). These geothermometers are based on temperature-depending mineral solubility (Fournier, 1977) or cation exchange reactions between mineral phases (Fournier, 1981; Arnórsson et al., 1983; Giggenbach, 1988). Both processes require mineral-fluid equilibrium and suppose that no mixing or re-equilibrium has occurred in water in their way from the reservoir up to the surface (Nicholson, 1993; Ellis, 1979; Fournier, 1977).

Samples for geothermometric analysis were selected with the K-Na-Mg geothermometer and geo-indicator (Fig. 11, Giggenbach, 1988, 1992). Five out of the ten thermal samples fall in the partial equilibrium field, indicating temperatures between 100 °C and 160 °C for the Na-K geothermometer, and up to 110 °C for the K–Mg geothermometer. These temperatures may be overestimated due to the absence of mica-chlorite alteration (used for the K/Mg geothermometer) in the study area. The partially equilibrated samples were used to calculate the Na-K-Ca (Fournier and Truesdell, 1973), Na/K (Arnórsson et al., 1983), the conductive chalcedony (Fournier, 1977), and the chalcedony saturation index (Reed and Spycher, 1984; calculated with PHREEQC using the phreeqc.dat database) geothermometers. The selection of these geothermometers was based upon the presence of plagioclase and alkaline feldspars in volcanic rocks, sericite and altered glass in sandstones (Webber et al., 1994; Lahiere, 1982), and silica in the outlet of springs and wells.

The calculated geothermometers yield temperatures ranges of 67–142 °C for the Na-K-Ca, 45–104 °C for the Na/K, 60–96 °C for the conductive chalcedony, and 57–94 °C for the chalcedony saturation index (Table 5, Fig. 12). The average equilibrium temperatures per sample define a range of 58 ± 9 °C to 102 ± 30 °C, in which most of the calculated values overlap (Fig. 12). The mean equilibrium temperatures per geothermometer range from 72 ± 16 °C to 88 ± 31 °C (Table 5, Fig. 12). The good agreement in the average temperatures suggests that the geothermometric results are reliable and imply a fast transportation method to bring fluids from the thermal reservoir to the surface without major chemical re-equilibration.

With these considerations, the low equilibrium temperatures (< 100 °C) suggest a shallow depth (2–3 km) for the hydrothermal reservoir in the Juchipila hydrothermal system, assuming an average geothermal gradient of 30 °C/km and air mean temperature of 22 °C in the area. Likewise, the radiogenic heat production of 0.49- 4.89 μWm^{-3} (calculated from U, Th, and K concentrations in some rocks from the basin; Martínez-Reséndiz, 2020) may account for an alternative/secondary water heating mechanism. This additional process

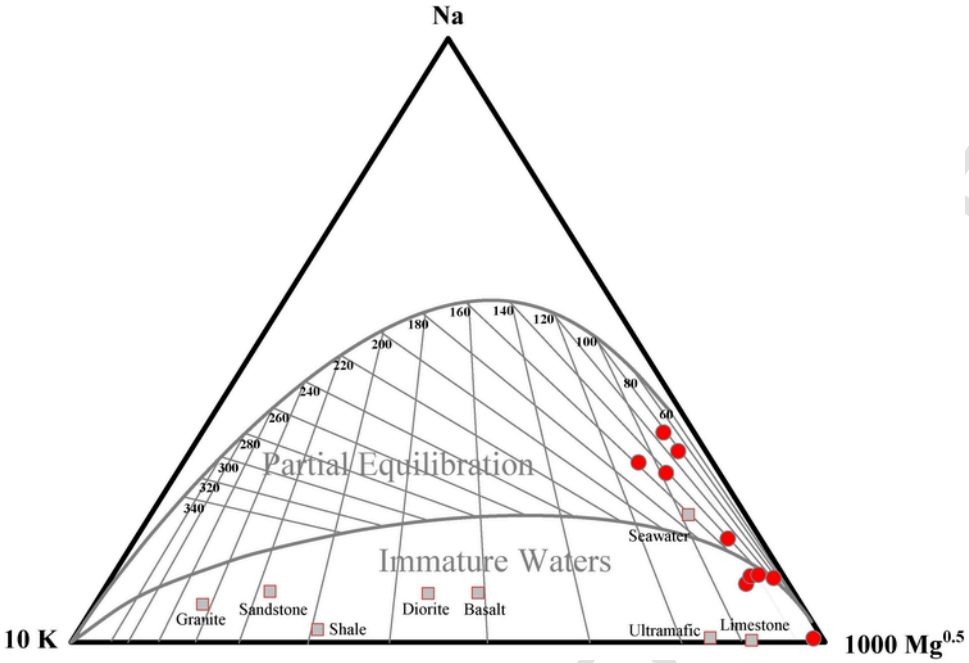

Fig. 11. K/100-Na/1000-$Mg^{1/2}$ ternary diagram and geothermometer (Giggenbach, 1988).

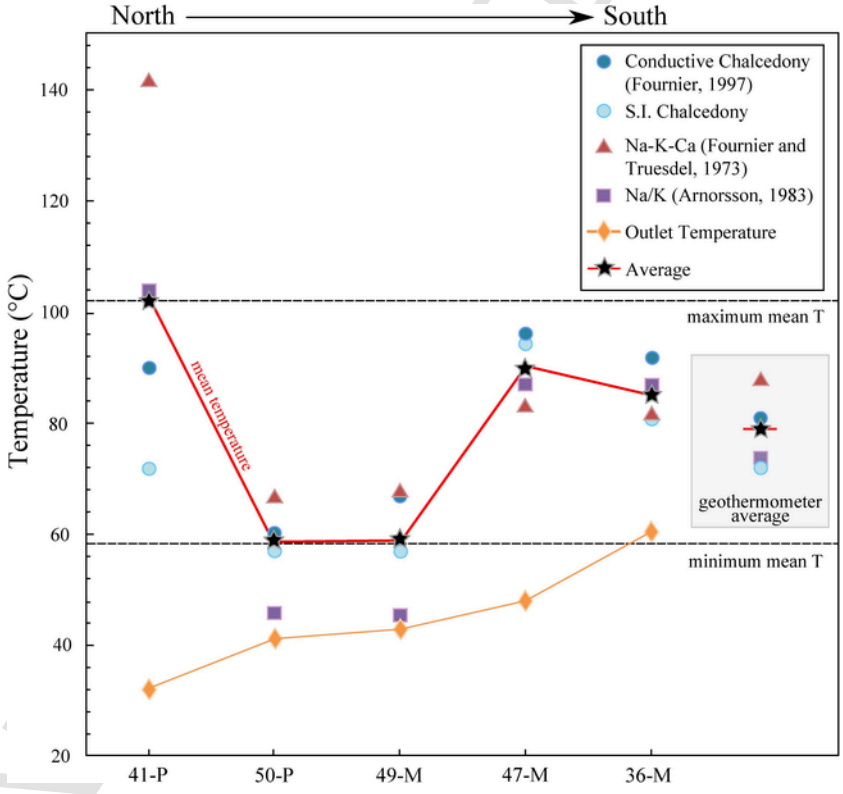

Fig. 12. Plot of outlet temperatures and solute geothermometers results for selected samples in the Juchipila Basin. Geothermometers: Na-K-Ca (Fournier and Truesdell, 1973), Na/K (Arnórsson et al., 1983), conductive chalcedony (Fournier, 1977), and the chalcedony saturation index (Reed and Spycher, 1984; calculated with PHREEQC using the phreeqc.dat database).

would increase the geothermal gradient, resulting in a shallower thermal reservoir. Further research on the volume and heat transfer mechanisms is needed to determine the extent of this contribution and its impact on the local geothermal gradient.

6. Conceptual model of the hydrothermal system

We present a conceptual model of the hydrothermal system in the Juchipila Basin in Fig. 13. In this model, the vertical recharge of the TW aquifer takes place in the high-altitude zones, mainly along the

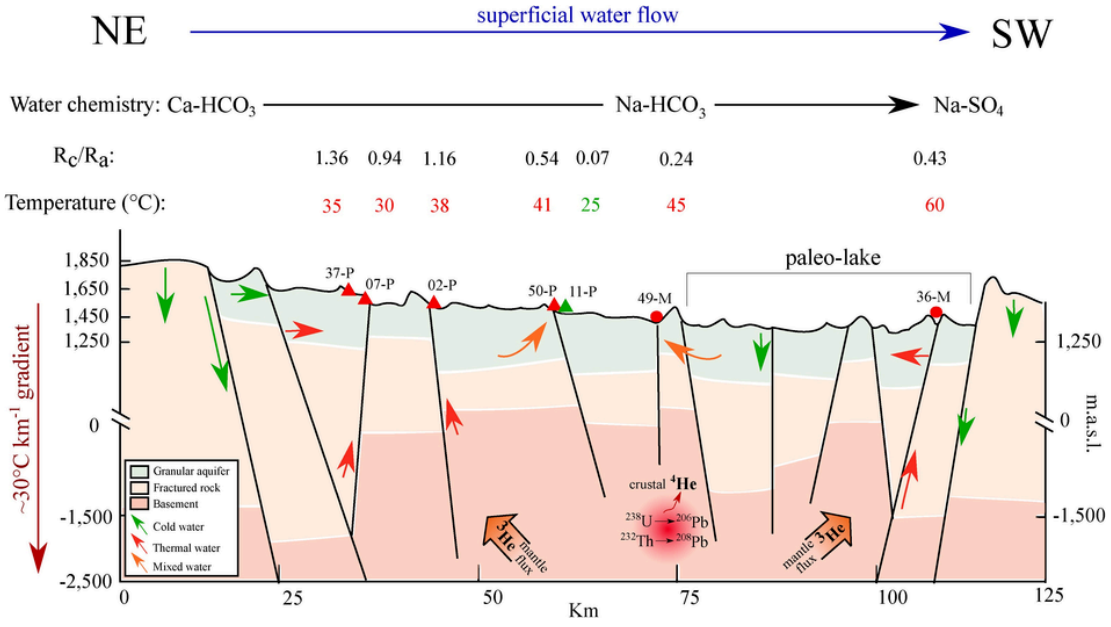

Fig. 13. Conceptual model of the hydrothermal system in the Juchipila Basin based on the magneto-telluric soundings of Avila Vargas (2019).

major faults bounding the graben (green downward arrows in Fig. 13). The natural forest cover (having a better infiltration capacity of soil), as well as the fractured ignimbrite and basalt along the fault damage zone, enhances the rapid infiltration of water in these areas. In agreement with the geothermometric mean temperatures range of 58 °C–102 °C and considering a minimum local geothermal gradient of ~30 °C/km, meteoric water travels through the fractured volcano-sedimentary succession reaching the basement, inferred to be a Cretaceous marine sedimentary succession, at 2–3 km depth (Martínez-Reséndiz, 2020). During the descent, groundwater dissolves minerals and groundmass from the volcano-sedimentary succession as it gets heated by the geothermal gradient; it also dissolves locally produced crustal helium, and incorporates mantle helium degassing from a deeper regional source.

In addition, another portion of the rainwater recharges the CW shallow granular aquifer, located in the sedimentary fill in the valley bottom (green downward arrows in Fig. 13). As a consequence of the agricultural land use and the local clay layers found in the sedimentary fill, this rainwater does not infiltrate rapidly and moves by gravity towards areas of lower elevation from north to south (superficial water flow direction arrow in Fig. 13). During this process of subsurface run-off, water evaporates before flowing to a deeper level in the granular aquifer where undergoes cation-exchange processes with soil and clay materials.

Although the TW aquifer dynamics is not properly characterized, we can assume the existence of hot water upwelling along high-permeability fault-associated pathways (red upward arrows in Fig. 13). During the return to the surface, hot water encounters the shallow cold aquifer, and the TW end-member mixes with the CW (orange arrows in Fig. 13), generating the whole range of chemical compositions (Ca–HCO_3 => Na–HCO_3 => Na-SO_4) depending on the local lithology and location in the basin.

7. Conclusions

In this study, we characterized the Juchipila low-temperature, unconventional geothermal reservoir using ion chemistry and O—H, He isotope characteristics. Thermal waters have either Na–HCO_3 and Na-SO_4 compositions and anomalous concentrations of Li, As, B, and F; the chemistry of this group is strongly controlled by the alteration and dissolution of the volcano-sedimentary succession in the basin. Cold waters have a Ca-Na–HCO_3 composition and anomalous concentration of NO_3; this group corresponds to the shallow granular aquifer in the valley experiencing cation-exchange processes and mixing with irrigation return flow.

Overall, the δ^2H–$\delta^{18}O$ isotope ratios (-79.3‰ to -53.2‰ for δ^2H and -10.8‰ to -6.3‰ for $\delta^{18}O$) in springs and groundwater indicate a common meteoric source but different recharge mechanisms for each group within the aquifer: a rapid vertical infiltration from precipitation, and a horizontal run-off of the cold waters enabling evaporation. Dissolved gases in thermal waters are mostly enriched in CO_2, and He with respect to the ASW, suggesting an interaction with non-atmospheric CO_2 and He. Helium in the Juchipila aquifer has mainly a crustal and an atmospheric source. However, the mantle contribution reaches up to 14 %, suggesting that the regional crustal fault systems at the boundary between the MC and SMO geologic provinces allow the up-flow of helium related to deep-seated gases and/or melts in the mantle.

The equilibrium temperatures calculated from solute geothermometry have mean values ranging from 58 to 102 °C. Taking into account the geologic and geophysical information available for the area, we propose that the hydrothermal system dynamics are controlled by crustal faults, related to the regional graben structures, suggesting the possibility of a potential regional energy reservoir. Rainwater recharging the graben edges travels through the fault system towards the fractured basement at 2–3 km deep. This water gets heated by the geothermal gradient while becoming enriched in ions and crustal and mantle helium, before returning to the surface through convective cells along regional faults and mixes with the cold, shallow aquifer.

These findings are useful to understand other magmatic-unrelated geothermal manifestations with similar geologic and tectonic settings, which altogether may contribute to estimating a more realistic geothermal potential for the area. The results of the dissolved helium isotope ratios in the waters of the Juchipila Basin have implications in the understanding of how large fault systems in central Mexico influence the hydrothermal fluid flow in the region. Although the Juchipila hydrothermal system may not be capable of producing electricity, other schemes of geothermal energy exploitation could be further explored to benefit the local communities.

Uncited references

.

CRediT authorship contribution statement

Andrea Billarent-Cedillo: Methodology, Validation, Writing - original draft. **Gilles Levresse:** Conceptualization, Methodology, Validation, Funding acquisition, Writing - original draft, Supervision. **Luca Ferrari:** Funding acquisition, Writing - original draft. **Claudio Inguaggiato:** Conceptualization, Methodology, Validation, Writing - original draft. **Salvatore Inguaggiato:** Methodology, Validation, Formal analysis. **Eliseo Hernandez-Pérez:** Validation, Formal analysis. **Antonio Hernández-Espriú:** Validation, Formal analysis, Funding acquisition, Writing - review & editing. **Fernando Corbo Camargo:** Methodology, Writing - review & editing. **Jaime Carrera Hernandez:** Methodology, Writing - review & editing. **Alberto Arias-Paz:** Validation, Formal analysis.

Declaration of Competing Interest

The authors report no declarations of interest.

Acknowledgments

This work was supported by the UNAM-DGAPA PAPIIT grant IV100117 (Centro de Geociencias and Facultad the Ingeniería, Hydrogeology Group, UNAM). Special thanks to Marina Vega, Carolina Muñoz Torres, Francisco Javier Otero Trujano, Edith Cienfuegos Alvarado, Javier Mancera Alejandrez, and Sergio Macías Medrano for their assistance at the laboratories. An acknowledgment to Alberto Arias-Paz, a former member of our research group, an excellent hydrogeologist, and a friend who passed away too early in October 2019, during the completion of this study. Thanks to Carlos Errázuriz for his help in the revision of text and figures. We thank the two anonymous reviewers for their constructive comments that gave us the opportunity to greatly improve the initial version.

Appendix A. Supplementary data

Supplementary material related to this article can be found, in the online version, at doi:https://doi.org/10.1016/j.geothermics.2021.102076.

References

Alarcón-Herrera, M.T., Bundschuh, J., Nath, B., Nicolli, H.B., Gutierrez, M., Reyes-Gomez, V.M., Nuñez, D., Martín-Dominguez, I.R., Sracek, O., 2013. Co-occurrence of arsenic and fluoride in groundwater of semi-arid regions in Latin America: genesis, mobility and remediation. J. Hazard. Mater. 262, 960–969. https://doi.org/10.1016/j.jhazmat.2012.08.005.

Appelo, C.A.J., Postma, D., 2005. Geochemistry, Groundwater and Pollution, 2nd edition CRC Press, Taylor & Francis Group, Boca Raton London New York.

Arnold, Y.P., Franco, G., Tassi, F., Caffe, P.J., Jofre, C., Claros, M., Cabassi, J., 2020. Geochemical features of hydrothermal systems in Jujuy Province, Argentina: hints for geothermal fluid exploration. J. South Am. Earth Sci.102627https://doi.org/10.1016/j.jsames.2020.102627.

Arnórsson, S., 2000. Isotopic and Chemical Techniques in Geothermal Exploration, Development and Use. International Atomic Energy Agency, Vienna, x 351. https://doi.org/10.1017/S0016756802267114.

Arnórsson, S., Gunnlaugsson, E., Svavarsson, H., 1983. The chemistry of geothermal waters in Iceland. III. Chemical geothermometry in geothermal investigations. Geochim. Cosmochim. Acta 47 (3), 567–577. https://doi.org/10.1016/0016-7037(83)90278-8.

Arnorsson, S., Stefansson, A., Bjarnason, J.O., 2007. Fluid-Fluid interactions in geothermal systems. Rev. Mineral. Geochem. 65 (1), 259–312. https://doi.org/10.2138/rmg.2007.65.9.

Arranda-Gomez, J.J., Luhr, J.F., Housh, T.B., Valdez-Moreno, G., Chavez-Cabello, G., Late Cenozoic intraplate-type volcanism in central and northern Mexico: A review. In Alaniz-Alvarez, S.A., and Nieto-Samaniego, A.F., eds., Geology of Mexico: Celebrating the Centenar of the Geological Society of Mexico: Geological Society of America Special paper 442, 2007, p. 93-128.Avila Vargas, O., 2019. Modelo del Graben de Juchipila a partir de datos magnetotelúricos. Master Thesis Universidad Nacional Autónoma de México, 345.

Batista Cruz, R.Y., Rizzo, A.L., Grassa, F., Bernard Romero, R., GonzálezFernández, A., Kretzschmar, T.G., Gómez-Arias, E., 2019. Mantle degassing through continental crust triggered by active faults: The case of the Baja California Peninsula, Mexico. Geochem. Geophys. Geosystems 20, 1912–1936. https://doi.org/10.1029/2018GC007987.

Battistel, M., Hurwitz, S., Evans, W., Barbieri, M., 2014. Multicomponent geothermometry applied to a medium-low enthalpy carbonate-evaporite geothermal reservoir. Energy Procedia 59, 359–365. https://doi.org/10.1016/j.egypro.2014.10.389.

Battistel, M., Hurwitz, S., Evans, C.W., Barbieri, M., 2016. The chemistry and isotopic composition of waters in the low-enthalpy geothermal system of Cimino-Vico Volcanic District, Italy. J. Volcanol. Geother. Res. 328, 222–229.

Beltrán-Martínez, B.C., 2019. Caracterización Geológico-Estructural de la Porción Norte del Graben de Juchipila, Estados de Zacatecas y Aguascalientes. Bachelor Thesis Universidad Autónoma de Guerrero.

Benson, B.B., Krause, D., 1980. Isotopic fractionation of helium during solution: a probe for the liquid state. J. Solution Chem. 9 (12), 895–909. https://doi.org/10.1007/BF00646402.

Böhlke, J.K., 2002. Groundwater recharge and agricultural contamination. Hydrogeol. J. 10 (1), 153–179. https://doi.org/10.1007/s10040-001-0183-3.

Boschetti, T., 2013. Oxygen isotope equilibrium in sulfate-water systems: a revision of geothermometric applications in low-enthalpy systems. J. Geochem. Explor. 124, 92–100. https://doi.org/10.1016/j.gexplo.2012.08.011.

Bruhn, D., Jolie, E., Kieling, K., Trumpy, E., Bonté, D., Liotta, D., Páll Hersir, G., Deb, P., van Wees, J.D., Huenges, E., 2020. GEMex: cooperation in geothermal energy research Europe-Mexico for development of enhanced geothermal systems and superhot geothermal systems. In: European Geothermal Congress 2019. Den Haag, The Netherlands, 11-14 June 2019.

Capasso, G., Inguaggiato, S., 1998. A simple method for the determination of dissolved gases in natural waters. An application to thermal waters from Vulcano Island. Appl. Geochem. 13 (5), 631–642. https://doi.org/10.1016/S0883-2927(97)00109-1.

Caracausi, A., Favara, R., Italiano, F., Paonita, A., Rizzo, A., Nuccio, P.M., 2004. Evidence of mantle derived fluid contributions to the thermal basins of Western Sicily: geotectonic and geodynamic implications. In: Eleventh International Symposium on Water-Rock Interaction Saratoga Spring. New York, USA. pp. 91–94.

Chadha, D.K., 1999. A proposed new diagram for geochemical classification of natural waters and interpretation of chemical data. Hydrogeol. J. 7 (5), 431–439. https://doi.org/10.1007/s100400050216.

CONAGUA, 2018. Actualización de la disponibilidad media anual de agua en el acuífero Jalpa-Juchipila (3209). Diaro Oficial de la Federación, Estado de Zacatecas.

Craig, H., 1961. Isotopic variations in meteoric waters. Science 133 (3465), 1702–1703.

Craig, H., Gordon, L.I., Horibe, Y., 1963. Isotopic exchange effects in the evaporation of water: 1. Low-temperature experimental results. J. Geophys. Res. 68 (17), 5079–5087.

Craig, H., Lupton, J.E., Welhan, J.A., Poreda, R., 1978. Helium isotope ratios in Yellowstone and Lassen Park volcanic gases. Geophys. Res. Lett. 5 (11), 897–900.

D'Amore, F., Arnórsson, S., 2000. Geothermometry. In: , Arnórsson S. (Ed.), Isotopic and Chemical Techniques in Geothermal Exploration, Development and Use. International Atomic Energy Agency, Vienna, pp. 152–199. https://doi.org/10.1017/S0016756802267114.

Delmelle, P., Bernard, A., 2015. The remarkable chemistry of sulfur in hyper-acid crater lakes: a scientific tribute to Bokuichiro Takano and Minoru Kusakabe. In: Rouwet, D., Christenson, B., Tassi, F., Vandemeulebrouck, J. (Eds.), Volcanic Lakes. pp. 239–258.

Ellis, A.J., 1979. Chemical geothermometry in geothermal systems. Chem. Geol. 25 (3), 219–226. https://doi.org/10.1016/0009-2541(79)90143-8.

Ferrari, L., Valencia-Moreno, M., Bryan, S., Alaniz-Álvarez, S.A., Nieto-Samaniego, Á.F., 2007. Magmatism and tectonics of the Sierra Madre Occidental and its relation with the evolution of the western margin of North America. Spec. Pap. Geol. Soc. Am. 422, 1. https://doi.org/10.1130/2007.2422(01).

Ferrari, L., López-Martínez, M., Orozco-Esquivel, T., Bryan, S.E., Duque-Trujillo, J., Lonsdale, P., Solari, L., 2013. Late Oligocene to Middle Miocene rifting and synextensional magmatism in the southwestern Sierra Madre Occidental, Mexico: the beginning of the Gulf of California rift. Geosphere 9 (5), 1161–1200.

Ferrari, L., Castillo-Reynoso, J.C., Orozco-Esquivel, T., Silva-Fragoso, A., 2018. Digital geologic map and geochronologic, geochemical and geothermal database of the south-eastern part of the Sierra Madre Occidental, Mexico. Terra Digitalis 2 (2).

Fischer, T.P., Chiodini, G., Volcanic, magmatic and hydrothermal gases. In: The encyclopedia of volcanoes, 2nd edn. Academic Press/Elsevier, Waltham, 2015, pp 779–796. https://doi.org/10.1016/B978-0-12-385938-9.00045-6 Fournier, R.O., 1977. Chemical geothermometers and mixing models for geothermal systems. Geothermics 5 (1-4), 41–50.

Fournier, R.O., 1981. Application of water geochemistry to geothermal exploration and reservoir engineering. In: Ryback, Muffler (Eds.), Geothermal Systems: Principles and Case Histories. John Wiley and Sons, NY, pp. 109–143.

Fournier, R.O., Truesdell, A.H., 1973. An empirical Na-K-Ca geothermometer for natural waters. Geochim. Cosmochim. Acta 37 (5), 1255–1275.

Fridleifsson, 2001. Geothermal energy for the benefit of the people. Renewable Sustainable Energy Rev. 5 (3), 299–312. https://doi.org/10.1016/S1364-0321(01)00002-00008.

Giggenbach, W.F., 1980. Geothermal gas equilibria. Geochim. Cosmochim. Acta 44 (12), 2021–2032.

Giggenbach, W.F., 1988. Geothermal solute equilibria. Geochemica et Cosmochemica Acta 52, 2749–2765.

Giggenbach, W.F., 1991. Chemical techniques in geothermal exploration. In: D'Amore, F. (Ed.), Application of Geochemistry in Geothermal Reservoir Development UNITAR/UNDP Centre on Small Energy Resources, Rome. pp. 119–144.

Giggenbach, W.F., 1992. Isotopic shifts in waters from geothermal and volcanic systems along convergent plate boundaries and their origin. Earth Planet. Sci. Lett. 113 (4), 495–510.

González-Guzmán, R., Inguaggiato, C., Peiffer, L., Weber, B., Kretzschmar, T., 2019. Fault-controlled geothermal fluids of the northern Trans-Mexican Volcanic Belt: A geochemical and isotopic study of the Los Geysers filed (Valley de Queretaro, Mexico). Journal of Volcanology and Geothermal Research, 388, 106681. Gutierrez-Negrin, L.C.A., Maya-Gonzalez, R., Quijano-Leon, J.L., 2015. Present situation and perspectives of geothermal in Mexico. In: Proceedings World Geothermal Congress 2015 Melbourne. Australia, 19-25 April 2015.

Gutiérrez-Negrín, L.C.A., 2019. Current status of geothermal-electric production in Mexico. In: Proceedings of 2nd International Geothermal Conference. IOP Conference Series: Earth and Environment Science. pp. 249–012017. https://doi.org/10.1088/1755-1315/249/1/012017.

Hermanska, M., Kleine, B.I., Stefansson, A., 2020. Geochemical constraints on supercritical fluids in geothermal systems. J. Volcanol. Geotherm. Res.106824https://doi.org/10.1016/j.jvolgeores.2020.106824.

Hilton, D.R., 1996. The helium and carbon isotope systematics of a continental geothermal system: results from monitoring studies at Long Valley caldera (California, U.S.A.). Chem. Geol. 127 (4), 269–295. https://doi.org/10.1016/0009-2541(95)00134-4.

Hooker, P.J., O'Nions, R.K., Oxburgh, E.R., 1985. Helium Isotopes in North Sea gas fields and the Rhine rift. Nature 53, 495–497. https://doi.org/10.1016/0016-7037(73)90060-4.

Inguaggiato, S., Rizzo, A., 2004. Dissolved helium isotope ratios in ground waters: a new technique based on gas–water re-equilibration and its application to Stromboli volcanic system. Appl. Geochem. 19 (5), 665–673. https://doi.org/10.1016/j.apgeochem.2003.10.009.

Inguaggiato, C., Censi, P., d'Alessandro, W., Zuddas, P., 2016. Geochemical characterisation of gases along the Dead Sea rift: evidences of mantle-CO_2 degassing. J. Volcanol. Geotherm. Res. 320, 50–57. https://doi.org/10.1016/j.jvolgeores.2016.04.008.

Inguaggiato, C., Burbano, V., Rouwet, D., Garzon, G., 2017. Geochemical processes assessed by rare earth elements fractionation at "Laguna Verde" acidic-sulphate crater lake (Azufral volcano, Colombia). Appl. Geochem. 79, 65–74. https://doi.org/10.1016/j.apgeochem.2017.02.013.

Inguaggiato, C., Vita, F., Diliberto, I.S., Calderone, L., 2017. The role of the aquifer in soil CO_2 degassing in volcanic peripheral areas: a case study of Stromboli island (Italy). Chem. Geol. 469, 110–116. https://doi.org/10.1016/j.chemgeo.2016.12.017.

Kennedy, B.M., van Soest, M.C., 2006. A helium isotope perspective on the Dixie Valley, Nevada, hydrothermal system. Geothermics 35 (1), 26–43. https://doi.org/10.1016/j.geothermics.2005.09.004.

Kennedy, B.M., van Soest, M.C., 2007. Flow of mantle fluids through the ductile lower crust: helium isotope trends. Science 318 (5855), 1433–1436. https://doi.org/10.1126/science.1147537.

, . . Cosmochim.

Kipfer, R., Aeschbach-Hertig, W., Peeters, F., Stute, M., 2002. Noble Gasesin Lakes and Ground waters. In: In: Porcelli, Donald, Ballentine, C.J., Wieler, R. (Eds.), Noble Gases in Geochemistry and Cosmochemistry Vol. 69, Mineralogical Society of America, Washington, DC, pp. 837–922, – ISBN 374;-8688\r2-;5;72-7;-8..

Kulongoski, J.T., Hilton, D.R., Barry, P.H., Esser, B.K., Hillegonds, D., Belitz, K., 2013. Volatile fluxes through the Big Bend section of the San Andreas Fault, California: helium and carbon-dioxide systematics. Chem. Geol. 339, 92–102. https://doi.org/10.1016/j.chemgeo.2012.09.007.

Lahiere, L., 1982. Petrology of Lacustrine Deposits, Juchipila Quadrangle, Zacatecas, Mexico. Unpublished Master Tesis Portland State University, Oregon, USA.

, .

Loza-Aguirre, I., Nieto-Samaniego, A.F., Alaniz-Álvarez, S.A., Iriondo, A., 2008. Relaciones estratigráfico-estructurales en la intersección del sistema de fallas San Luis-Tepehuanes y el graben de Aguascalientes, México central. Revista Mexicana de Ciencias Geológicas 25 (3), 533–548.

Lund, J.W., Freeston, D.H., Boyd, T.L., 2005. Direct application of geothermal energy: 2005 worldwide review. Geothermics 34 (6), 691–727.

, .

Martínez-Reséndiz, E.V., 2020. Estudio geológico del sector centro y sur del graben de Juchipila, Jal., Zac., México. Master Thesis Universidad Nacional Autónoma de México.

Méjean, P., Pinti, D. L., Kagoshima, T., Roulleau, E., Demarets, L., Poirier, A., Takahata, N., Sano Y., Larocque, M., 2020. Mantle helium in Southern Quebec groundwater: A possible fossil record of the New England hotspot. Earth and Planetary Science Letters, 545, 116352. Mifflin, M.D., 1988. Region 5, Great Basin. Hydrogeology. The Geological Society of North America, Boulder Colorado, 69–78.

Morales-Arredondo, J.I., Esteller-Alberich, M.V., Armienta Hernández, M.A., Martínez-Florentino, T.A.K., 2018. Characterizing the hydrogeochemistry of two low-temperature thermal systems in Central Mexico. J. Geochem. Explor. 185, 93–104. https://doi.org/10.1016/j.gexplo.2017.11.006.

Nicholson, K., 1993. Geothermal Fluids. Springer Berlin Heidelberg, Berlin, Heidelberg, https://doi.org/10.1007/978-3-642-77844-5.

Nicolli, H.B., Bundschuh, J., Blanco, M.C., Tujchneider, O.C., Panarello, H.O., Dapeña, C., Rusansky, J.E., 2012. Arsenic and associated trace-elements in groundwater from the Chaco-Pampean plain, Argentina: results from 100 years of research. Sci. Total Environ. 429, 36–56. https://doi.org/10.1016/j.scitotenv.2012.04.048.

Nieto-Samaniego, Á.F., Ferrari, L., Alaniz-Alvarez, S.A., 1999. Variation of Cenozoic extension and volcanism across the southern Sierra Madre Occidental volcanic province, Mexico. Geol. Soc. Am. Bull. 17, 347–363. https://doi.org/10.1130/0016-7606(1999)111<0347:VOCEAV>2.3.CO2.

Nieto-Samaniego, Ángel F., Alaniz-Alvarez, S.A., Camprubí, A., 2005. La Mesa Central de México: estratigrafía, estructura y evolución tectónica cenozoica. Boletín de la Sociedad Geológica Mexicana LVII 3, 285–318.

Norman, D.I., Moore, J.N., 1999. Methane and excess N_2 and Ar in geothermal fluid inclusions. In: Stanford University, Stanford, California. Proceedings: Twenty-Fourth Workshop of Geothermal Reservoir Engineering, vol. 22, p. 24.

Paz-Pérez, A., 2019. Caracterización hidrogeológica del graben de Juchipila e implicaciones geotérmicas. Unpublished licence thesis Universidad Nacional Autónoma de México, 101.

Pinti, D.L., Castro, M.C., Shouakar-Stash, O., Tremblay, A., Garduño, V.H., Hall, C.M., Ghaleb, B., 2013. Evolution of the geothermal fluids at Los Azufres, Mexico, as traced by noble gas isotopes, $\delta^{18}O$, δD, $\delta^{13}C$ and $^{87}Sr/^{86}Sr$. J. Volcanol. Geotherm. Res. 249, 1–11. https://doi.org/10.1016/j.jvolgeores.2012.09.006.

Pinti, D.L., Castro, M.C., López-Hernández, A., Hernández, M.A.H., Richard, L., Hall, C.M., Rodríguez-Rodríguez, M.H., 2019. Cerro Prieto geothermal field (Baja California, Mexico)–a fossil system? Insights from a noble gas study. J. Volcanol. Geotherm. Res. 371, 32–45.

Reed, M., Spycher, N., 1984. Calculation of pH and mineral equilibria in hydrauthermal waters with application to geothermometry and studies of boiling and dilution. Geochemica et Cosmochemica Acta, 48, 1479-1492. Rizzo, A.L., Barberi, F., Carapezza, M.L., Di Piazza, A., Francalanci, L., Sortino, F., D'Alessandro, W., 2015. New mafic magma refilling a quiescent volcano: evidence from He-Ne-Ar isotopes during the 2011–2012 unrest at Santorini, Greece. Geochem. Geophys. Geosyst. 16 (3), 798–814. https://doi.org/10.1002/2014GC005653.

Rodvang, S.J., Mikalson, D.M., Ryan, M.C., 2004. Changes in ground water quality in an irrigated area of Southern Alberta. J. Environ. Qual. 33, 476–487. https://doi.org/10.2134/jeq2004.4760.

, . –

Sano, Y., Wakita, H., 1985. Geographical distribution of $^3He/^4He$ ratios in Japan: Implications for arc tectonics and incipient magmatism. J. Geophys. Res. 90 (B10), 8729–8741. https://doi.org/10.1029/JB090iB10p08729.

Shaw, D.M., Sturchio, N.C., 1992. Boron-lithium relationships in rhyolites and associated thermal waters of young silicic calderas, with comments on incompatible element behaviour. Geochim. Cosmochim. Acta 56 (10), 3723–3731. https://doi.org/10.1016/0016-7037(92)90165-F.

Smith, S. P., & Kennedy, B. M., The solubility of noble gases in water and in NaCl brine. Geochim. Cosmochim. Acta, 47(3), 1983, 503-515. Spycher, N., Sonnenthal, E., Kennedy, B.M., 2011. Integrating multicomponent chemical geothermometry with parameter estimation computations for geothermal exploration. Trans. Geother. Res. Counc. Vol. 35 (1), 663–666.

Straub, S.M., Gomez-Tuena, A., Stuart, F.M., Zellmer, G.F., Espinasa-Perena, R., Cai, Y., Iizuka, Y., 2011. Formation of hybrid arc andesites beneath thick continental crust. Earth Planet. Sci. Lett. 303 (3-4), 337–347.

Torgersen, T., Jenkins, W.J., 1982. Helium isotopes in geothermal systems: Iceland, the geysers, raft river and steamboat springs. Geochim. Cosmochim. Acta 46 (5), 739–748. https://doi.org/10.1016/0016-7037(82)90025-4.

Torgersen, T., Drenkard, S., Stute, M., Schlosser, P., Shapiro, A., 1995. Mantle helium in ground waters of eastern North America: Time and space constraints on sources. Geology, 23(8), 675-678. Tóth, J., 1999. Groundwater as a geologic agent: an overview of the causes, processes, and manifestations. Hydrogeol. J. 7 (1), 1–14. https://doi.org/10.1007/s100400050176.

Wassenaar, L.I., Van Wilgenburg, S.L., Larson, K., Hobson, K.A., 2009. A groundwater isoscape (δD, $\delta^{18}O$) for Mexico. J. Geochem. Explor. 102 (3), 123–136. https://doi.org/10.1016/j.gexplo.2009.01.001.

Webber, K., Fernandez, L., Simons, W., 1994. Geochemistry and mineralogy of the eocene-oligocene volcanic sequence, Southern Sierra Madre Occidental, Juchipila, Zacatecas, Mexico. Geofísica Internacional 33 (1), 77–89. https://doi.org/10.22201/igeof.00167169p.1994.33.1.541.

, .

Wolaver, B.D., Crossey, L.J., Karlstrom, K.E., Banner, J.L., Cardenas, M.B., Ojeda, C.G., Sharp, J.M., 2013. Identifying origins of and pathways for spring waters in a semiarid basin using He, Sr, and C isotopes: Cuatrocienegas Basin, Mexico. Geosphere 9 (1), 113–125. https://doi.org/10.1130/GES00849.1.